

# Neutrino-Oxygen $CC0\pi$ scattering in the SuSAv2-MEC model

G.D. Megias<sup>a</sup>, M.B. Barbaro<sup>b</sup>, J.A. Caballero<sup>a</sup>, J.E. Amaro<sup>c</sup>,

T.W. Donnelly<sup>d</sup>, I. Ruiz Simo<sup>c</sup>, J. W. Van Orden<sup>e,f</sup>

<sup>a</sup>*Departamento de Física Atómica, Molecular y Nuclear,  
Universidad de Sevilla, 41080 Sevilla, Spain*

<sup>b</sup>*Dipartimento di Fisica, Università di Torino and INFN,  
Sezione di Torino, Via P. Giuria 1, 10125 Torino, Italy*

<sup>c</sup>*Departamento de Física Atómica, Molecular y Nuclear,  
and Instituto de Física Teórica y Computacional Carlos I,  
Universidad de Granada, Granada 18071, Spain*

<sup>d</sup>*Center for Theoretical Physics, Laboratory for Nuclear Science and Department of Physics,  
Massachusetts Institute of Technology,  
Cambridge, Massachusetts 02139, USA*

<sup>e</sup>*Department of Physics, Old Dominion University, Norfolk, Virginia 23529, USA and*

<sup>f</sup>*Jefferson Laboratory, 12000 Jefferson Avenue,  
Newport News, Virginia 23606, USA\**

(Dated: April 22, 2019)

arXiv:1711.00771v1 [nucl-th] 2 Nov 2017

---

\* Notice: Authored by Jefferson Science Associates, LLC under U.S. DOE Contract No. DE-AC05-06OR23177. The U.S. Government retains a non-exclusive, paid-up, irrevocable, world-wide license to publish or reproduce this manuscript for U.S. Government purposes

## Abstract

We present the predictions of the SuSAv2-MEC model for the double differential charged-current muonic neutrino (antineutrino) cross section on water for the T2K neutrino (antineutrino) beam. We validate our model by comparing with the available inclusive electron scattering data on oxygen and compare our predictions with the recent T2K  $\nu_\mu$ - $^{16}\text{O}$  data [1], finding good agreement at all kinematics. We show that the results are very similar to those obtained for  $\nu_\mu$ - $^{12}\text{C}$  scattering, except at low energies, and we comment on the origin of this difference. A factorized spectral function model of  $^{16}\text{O}$  is also included for purposes of comparison.

PACS numbers: 13.15.+g, 25.30.Pt

## I. INTRODUCTION

The accurate understanding of medium effects in neutrino-nucleus scattering has become a major challenge in recent years due to the essential role played by nuclear physics in the analysis of neutrino oscillation experiments. In fact, nuclear modeling uncertainties for this process represent the main source of systematic error for present (T2K, NOvA) and future (HyperK, DUNE) long baseline neutrino experiments, aiming at precision measurements of neutrino oscillation parameters and searching for leptonic CP violation. This has triggered intense activity in the nuclear theory community with the goal of describing neutrino-nucleus observables with high accuracy [2–17].

Most of the past work was focused on scattering of neutrinos and antineutrinos on mineral oil,  $\text{CH}_2$ , which has been the most commonly used target up to now. However, there is increasing interest in theoretical predictions for cross sections on different targets, specifically  $^{40}\text{Ar}$  and  $^{16}\text{O}$ . In particular, in the T2K experiment the far detector may have different nuclear targets, mineral oil and water, and it is then crucial to understand how to extrapolate the results from one target to another.

The aim of this paper is, within the framework of the SuSAv2-MEC nuclear model [9, 16, 18], to explore the similarities and differences between charged current (CC) (anti)neutrino scattering with no pions in the final state (the so-called  $\text{CC}0\pi$  process) on  $^{16}\text{O}$  and  $^{12}\text{C}$ . This process receives contributions from two different reaction mechanisms: quasielastic (QE) scattering, where the probe couples to the one-body current of a single bound nucleon, and the process where scattering occurs on a pair of nucleons interacting through the exchange of a meson, giving rise to two-body meson exchange currents (MEC). These two mechanisms in general have different dependences on the nuclear species, namely they scale differently with the nuclear density [19]. Therefore a careful investigation of this behavior for the two contributions must be performed before extrapolating the results from one nucleus to another.

A further difficulty arises from the fact that in oscillation experiments the neutrino energy is not known precisely, but broadly distributed around a maximum value: as a consequence each kinematic situation for a given outgoing lepton corresponds to a range of different neutrino energies and the one- and two-body responses cannot be disentangled in the experimental data. The situation is different in electron scattering, where the very precise

knowledge of energy and momentum transfer allows one to identify clearly the different reaction mechanisms. As a consequence,  $(e, e')$  data provide a necessary test for the validity of the nuclear model.

The paper is organized as follows: in Sec. II we introduce the basic formalism and briefly review the SuSAv2+MEC model. In Sec. III we present our results: we validate the model by comparing with inclusive electron scattering data on  $^{16}\text{O}$  (Sec. III A), we show our predictions for the T2K  $\text{CC}0\pi$  cross section on  $^{16}\text{O}$  and compare with recent data [1] (Sect. III B), intercompare the results on  $^{12}\text{C}$  and  $^{16}\text{O}$  (Sec. III C) and present predictions for antineutrinos on oxygen and water in Sec. III D. A factorized spectral function model [20–22] for  $^{16}\text{O}$  is shown for purposes of comparison. Finally, in Sec. IV we draw our conclusions.

## II. THEORETICAL FORMALISM: THE MODEL

The general formalism describing electron and charged-current neutrino-nucleus scattering processes has already been presented in detail in previous works [15, 16, 23–27]. Here we summarize the basic expressions involved in the differential cross sections for the discussion that follows. In the case of electron scattering, the double differential  $(e, e')$  inclusive cross section is given in terms of two response functions that account for all of the information on the nuclear effects involved in the process,

$$\frac{d^2\sigma}{d\Omega_e d\omega} = \sigma_{Mott} \left[ v_L R^L(q, \omega) + v_T R^T(q, \omega) \right], \quad (1)$$

where  $\sigma_{Mott}$  is the Mott cross section and the  $v$ 's are kinematical factors that only depend on the leptonic variables (see [28] for their explicit expressions). The response functions are given by  $R^{L,T}$  with  $L$  ( $T$ ) referring to the longitudinal (transverse) direction of the transferred momentum,  $q$ . Notice that both responses contain isoscalar and isovector contributions.

In the case of CC neutrino-nucleus scattering, the double differential cross section is also decomposed in a sum of responses, each of them composed of pure vector (VV), axial (AA) and interference (VA) components. The general expression for the cross section is given by

$$\frac{d\sigma}{dk' d\Omega} = \sigma_0 \left[ \hat{V}_{CC} \hat{R}^{CC} + 2\hat{V}_{CL} \hat{R}^{CL} + \hat{V}_{LL} \hat{R}^{LL} + \hat{V}_T \hat{R}^T \pm 2\hat{V}_{T'} \hat{R}^{T'} \right], \quad (2)$$

with  $\hat{R}^K$  the weak nuclear response functions, and

$$\sigma_0 = \frac{G_F^2 \cos^2 \theta_c}{2\pi^2} \left( k' \cos \frac{\tilde{\theta}}{2} \right)^2, \quad (3)$$

that depends on the Fermi constant  $G_F$ , the Cabibbo angle  $\theta_c$ , the outgoing lepton momentum  $k'$ , and the generalized scattering angle  $\tilde{\theta}$  [15]. The terms  $\hat{V}_K$  are kinematical factors whose explicit expressions can be found in [15, 29]. Note that the transverse channel contains an interference vector-axial (VA) response that is constructive (+) for neutrino scattering and destructive (−) for antineutrinos.

### A. SuSAv2: brief summary

In this work all the electromagnetic and weak nuclear responses have been evaluated within the framework of the SuSAv2 model [16]. This approach, based on the scaling and superscaling properties exhibited by electron scattering data, also takes into account the behavior of the responses provided by the Relativistic Mean Field (RMF). Contrary to the original SuSA model where a unique phenomenological scaling function, extracted from the analysis of the longitudinal response data for electron scattering, is used for both longitudinal and transverse electromagnetic responses as well as for all the weak neutrino responses, SuSAv2 is constructed by accounting for RMF effects and a separate analysis of the isovector and isoscalar channels. Thus the natural enhancement of the transverse electromagnetic response provided by RMF, a genuine dynamical relativistic effect, is incorporated in the SuSAv2 approach. However, in spite of the undeniable merits of the RMF description, *i.e.*, it provides a scaling function with the right asymmetry (tail extended to high values of the energy transferred  $\omega$ ) and a transverse scaling function that exceeds by  $\sim 20\%$  the longitudinal one, RMF predictions do not behave properly at high values of the momentum transfer  $q$ . In particular, the RMF peak position and the asymmetry of the scaling function keep growing with  $q$ . This is a consequence of the strong energy-independent scalar and vector potentials involved in the RMF. Hence, while the RMF approach works properly at low to intermediate values of  $q$ , where the effects linked to the treatment of the final-state interactions (FSI) are significant, it clearly fails at higher  $q$  where FSI become less and less important and the relativistic plane-wave impulse approximation (RPWIA) much more appropriate. Both approaches, RMF and RPWIA, are incorporated in the SuSAv2 model by using scaling functions that are given as linear combinations of the RMF and RPWIA predictions with a  $q$ -dependent “blending” function that allows a smooth transition from low to intermediate  $q$ -values (validity of RMF) to high  $q$  (RPWIA-based region).

Although SuSAv2 was originally applied to the analysis of data within the quasielastic (QE) domain, *i.e.*, based on the validity of the impulse approximation (IA), in [9] the model was extended also to the inelastic region by employing phenomenological fits to the single-nucleon inelastic electromagnetic structure functions. Notice that in both regimes, QE and inelastic, the general structure of the “blending” scaling functions is similar, and the difference in the nuclear responses comes essentially from the single-nucleon structure functions used, elastic versus inelastic, as well as from the different region ( $q, \omega$ -values) explored. The sensitivity of the model to several choices of the parameters involved in the “blending” function as well as a detailed comparison between the SuSAv2 predictions and inclusive ( $e, e'$ ) data on  $^{12}\text{C}$  for very different kinematical situations was presented in [9]. In the case of  $^{16}\text{O}$  the available electron scattering data cover only a limited kinematic region (see [30] and [31]) and can be well represented using constant parameters, specifically a Fermi momentum  $k_F=230$  MeV/ $c$  and an energy shift  $E_{shift}=16$  MeV, as discussed below. In order to apply the model to the wider kinematic range of interest in neutrino experiments, we assume the same  $q$ -dependence of the parameters found by fitting the carbon data, with a global rescaling of the Fermi momentum and energy shift to the values above specified. This choice is motivated by the validity of second-kind scaling, which is fulfilled very well by electron scattering data on different nuclei.

The SuSAv2 model, with the separate analysis of the isoscalar and isovector channels, makes it very well suited for describing charged-current (CC) neutrino-nucleus scattering processes. This has been clearly illustrated in [16] where the model was applied to CC neutrino reactions within the QE domain. Furthermore, its extension to the inelastic region was introduced in [18], but restricting the analysis to the  $\Delta$  resonance that in most of the cases plays a major role. The addition of higher inelasticities is in progress and the results will be presented in a forthcoming publication.

## B. 2p-2h MEC responses

Ingredients beyond the IA, namely 2p-2h MEC effects, have been shown to play a very significant role in the “dip” region between the QE and  $\Delta$  peaks. This has clearly been illustrated in [9] where the 2p-2h MEC effects added to the SuSAv2 predictions (denoted as SuSAv2-MEC) provide a very good description of inclusive ( $e, e'$ ) data on  $^{12}\text{C}$  covering the

entire energy spectrum at very different kinematics. Contrary to the SuSAv2 approach, that is largely based on the phenomenology of electron scattering data, although also inspired by the RMF predictions in the QE domain, the 2p-2h MEC calculations are entirely performed within the Relativistic Fermi Gas (RFG) model. This is due to the technical difficulties inherent to the calculation of relativistic two-body contributions even in the simple RFG model. However, it is noteworthy to point out that the present 2p-2h MEC contributions correspond to a fully relativistic calculation, needed for the extended kinematics involved in neutrino reactions. Moreover, all the electromagnetic (longitudinal and transverse) as well as the whole set of weak responses, including the vector, axial and axial-vector interference contributions in all channels have been evaluated exactly, that is, no particular assumption on the behavior and/or magnitude of any response has been considered. In order to apply the present calculation to the analysis of current and future neutrino oscillation experiments, with its possible implementation into the Monte Carlo generators, we have developed a parametrization of the MEC responses in the range of momentum transfer  $q = 50, \dots, 2000$  MeV/c, that significantly reduces the computational time. Its functional form is given in detail in [9, 18] for the case of  $^{12}\text{C}$ , and here it is extended to the analysis of  $^{16}\text{O}$  data.

### C. Oxygen versus Carbon predictions

Some comments are in order concerning the present results for  $^{16}\text{O}$  compared with the previous ones for  $^{12}\text{C}$  (see [9, 18]). In the particular case of the SuSAv2 model, no differences in the scaling functions are assumed for the two nuclei, except for the values used for the Fermi momentum and energy shift:  $k_F = 228$  MeV/c,  $E_{shift} = 20$  MeV for  $^{12}\text{C}$  and  $k_F = 230$  MeV/c,  $E_{shift} = 16$  MeV for  $^{16}\text{O}$ . These values are in accordance with the ones considered in [9, 18, 32] for  $^{12}\text{C}$ . In the case of  $^{16}\text{O}$ , the  $k_F$  and  $E_{shift}$ -values selected are also consistent with the general trend observed in [32]. This is at variance with some previous works [24, 29, 33, 34] where  $^{16}\text{O}$  was described by using  $k_F = 216$  MeV/c and  $E_{shift} = 25$  MeV. Although the two sets of values only lead to small differences in the cross sections (see below), the present choice does provide a more consistent analysis, and more importantly, it also improves the comparison with electron scattering data. The use of the same scaling functions for both nuclear systems is consistent with the property of scaling of second kind, *i.e.* independence of the scaling function with the nucleus, and it also follows

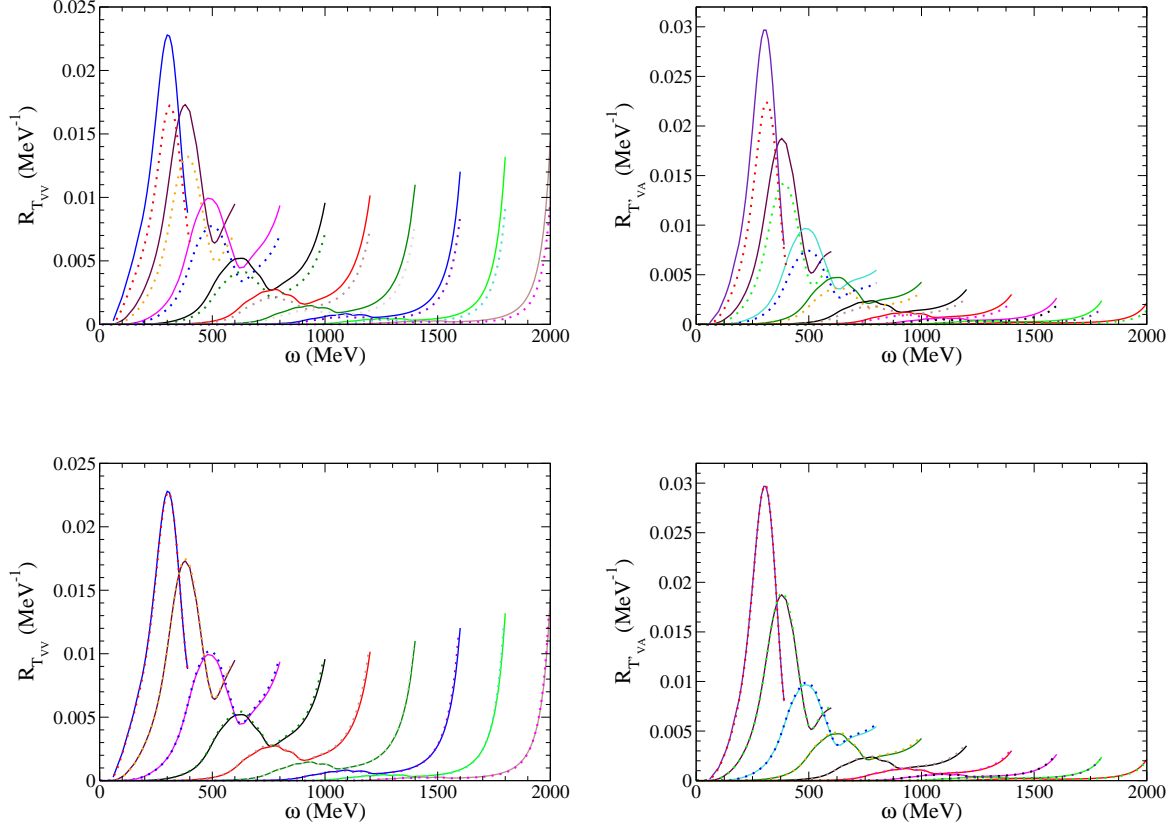


FIG. 1: (Color online) 2p-2h MEC vector-vector transverse ( $T_{VV}$ ) response and the axial-vector interference ( $T'_{VA}$ ) one. Comparison between the results for  $^{12}\text{C}$  (dots) and  $^{16}\text{O}$  (solid). Bottom panels: comparison by re-scaling the  $^{12}\text{C}$  results with a factor 1.35 (see text). The curves are displayed from left to right in steps of  $q = 200$  MeV/ $c$ , starting at  $q = 400$  MeV/ $c$

from the theoretical predictions provided by the RMF and RPWIA models on which SuSAv2 relies. This has been studied in detail in previous works (see [14, 33, 35, 36]) where the electromagnetic and weak scaling functions evaluated with the RMF and RPWIA approaches have been compared for  $^{12}\text{C}$  and  $^{16}\text{O}$ . Although the two models lead to significant differences, with the asymmetry (long tail extended at high  $\omega$ -values) only emerging when FSI are accounted for through the strong energy-independent scalar and vector potentials that are present in the RMF model, only very minor differences appear in the inter-comparisons for the two nuclei.

Regarding the 2p-2h MEC contributions, our calculations show that they approximately scale as  $k_F^2$ . This result, that is consistent with some analyses presented in the past [37, 38],

also matches the detailed study we have recently pursued in [19]. However, it is important to point out that, although the  $k_F^2$ -scale rule for the MEC responses works remarkably well at the peak of the MEC response (see [19]), the degree of its validity depends on the particular region explored. In the present analysis, we have checked that the same parametrization already considered for  $^{12}\text{C}$  can be extended to  $^{16}\text{O}$  but re-scaled with a factor 1.35, that is close to the ratio  $8/6 [k_F(O)/k_F(C)]^2$  between the nucleon numbers and the squares of the Fermi momenta for the two nuclei, and taking into account the different energy shifts. This provides the best fit of the fully relativistic results for  $^{16}\text{O}$ . These results are presented in Fig. 1 where two of the MEC responses are shown for the two nuclear systems (top panels), and their comparison when using the re-scale factor (bottom panels). Note the degree of accuracy between the results for both nuclei. Similar comments also apply to all the remaining electromagnetic and weak responses (not shown for brevity).

### III. RESULTS

In what follows we apply our SuSAv2-MEC model to electron and CC neutrino scattering reactions on  $^{16}\text{O}$  and compare the theoretical predictions with data taken at different kinematics and, in the case of neutrinos, given by the T2K collaboration [1]. The discussion follows closely the analysis already presented in the case of  $^{12}\text{C}$  for electron [9] and neutrino (antineutrino) [18] processes, where data are given in [39–41].

#### A. Electron scattering

Any theoretical model that aspires to describe neutrino-nucleus scattering processes should be first tested against electron scattering data. Thus a consistent description of electron scattering cross sections including not only the QE regime but also higher energy transfer regions (nucleon resonances and inelastic spectrum) is essential for the analysis of current neutrino oscillation experiments. Following our previous study on  $^{12}\text{C}$  [9], here we apply the SuSAv2-MEC model to  $^{16}\text{O}$  for which the amount of available ( $e, e'$ ) experimental data is, unfortunately, much smaller (see <http://faculty.virginia.edu/qes-archive/> and [42]). We employ the Gari-Krumpelmann (GKex) model for the elastic electromagnetic form factors [43], whereas the inelastic structure functions are described making use of the Bosted

and Christy parametrization [44]. The contribution of the 2p-2h MEC is also included in both the longitudinal and transverse channels. In accordance with previous comments, the value of the Fermi momentum is fixed to  $k_F = 230$  MeV/c.

In Fig. 2 our predictions are compared with data for six different kinematical situations, corresponding to all the available  $^{16}\text{O}$  data. In all the cases we present the separate contributions for the QE, 2p-2h MEC and inelastic regimes. The inclusive cross sections are given versus the transferred energy ( $\omega$ ), and each panel corresponds to fixed values of the incident electron energy ( $E_i$ ) and the scattering angle ( $\theta$ ). Whereas the latter is fixed to  $32^\circ$  [30] except for one case (center panel on the top, *i.e.*,  $\theta = 37.1^\circ$ ) [31], the electron energy values run from 700 MeV (left-top panel), where the QE peak dominates, to 1500 MeV (right-bottom) with the inelastic channel providing a very significant contribution. This is due to the values of the transferred momentum  $q$  involved in each situation. Although  $q$  is not fixed in each of the panels, *i.e.*, it varies as  $\omega$  also varies, the range of  $q$ -values allowed by the kinematics increases very significantly as the electron energy grows (for fixed scattering angles). Thus, for higher  $E_i$  the two regimes, QE and inelastic, overlap strongly, the inelastic processes being responsible for the large cross sections at increasing values of  $\omega$ . This different range of  $q$ -values spanned in each panel also explains the relative role played by the RMF versus the RPWIA approaches. Although not shown in the figure for sake of clarity, whereas the RMF response dominates at lower  $E_i$ -values (panels from left to right on the top), the reverse occurs, that is, the scaling function is essentially given by the RPWIA prediction, as  $E_i$  increases (panels on the bottom).

As observed, the SuSAv2-MEC predictions are in very good accordance with data for all kinematical situations. Although the relative role of the 2p2h-MEC effects is rather modest compared with the QE and inelastic contributions, its maximum is located in the dip region between the QE and inelastic peaks. This makes 2p2h-MEC essential in order to describe successfully the behavior of  $(e, e')$  data against the transferred energy  $\omega$ . This is clearly illustrated for all the panels in Fig. 2. Data in the dip region can only be reproduced by adding MEC effects to the tails of the QE and inelastic curves. Indeed, at the peak of the 2p2h response the three contributions are comparable in size.

The spectral function model, as used here, is described in more detail in [22] for semi-inclusive  $\text{CC}\nu$  scattering on  $^{16}\text{O}$ . It is factorized with the relativistic single-nucleon cross section folded with a non-relativistic spectral function [20, 21]. It contains the correct rel-

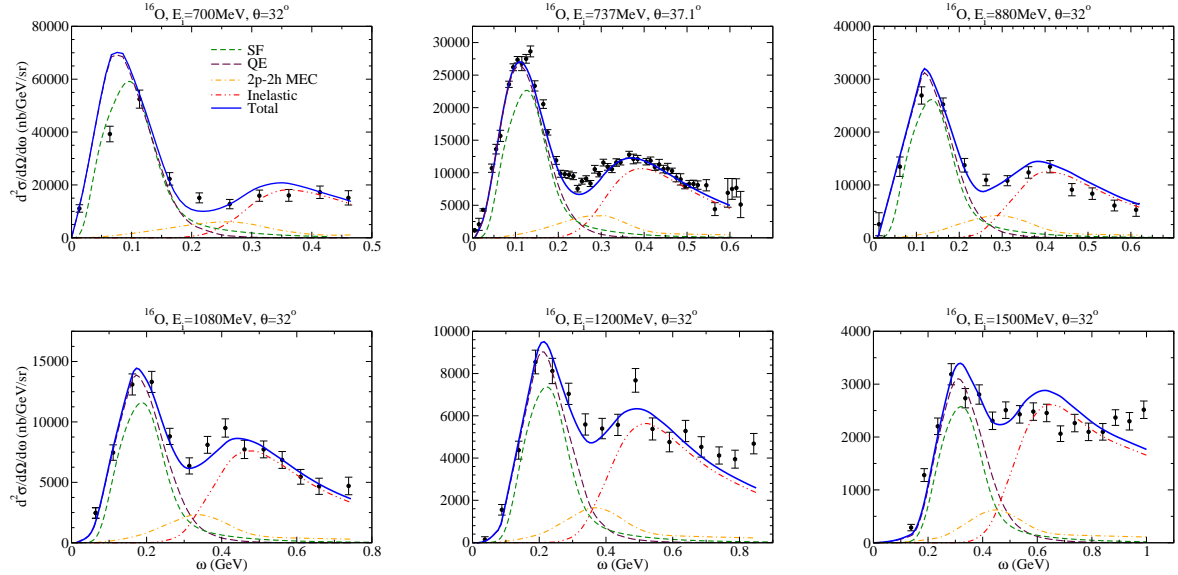


FIG. 2: (Color online) Comparison of inclusive  $^{16}\text{O}(e, e')$  cross sections and predictions of the SuSAv2-MEC model. The separate contributions of the pure QE response (dashed violet line), the 2p-2h MEC (dot-dashed), inelastic (double-dot dashed) are displayed. The sum of the three contributions is represented with a solid blue line. The spectral function (SF) result for the QE cross section is also shown for comparison (dashed green curve). The data are from [30] and [31].

ativistic kinematics, but since it is essentially rooted in PWIA it contains no transverse enhancement as in SuSAv2 approach and has no two-body MEC or meson production contributions. Its magnitude is therefore generally somewhat smaller than the SuSAv2 QE contribution and differs slightly in the position of the QE peak. This said, it is encouraging that the SF and SuSAv2 results for the QE contributions are not dramatically different. This result is in line with what was shown in [45] for the case of neutral current Neutrino-Oxygen scattering.

## B. T2K neutrino $^{-16}\text{O}$ scattering

Results for CC neutrino reactions on  $^{16}\text{O}$  are shown in Fig. 3. Each panel presents the double differential cross section averaged over the T2K muonic neutrino flux versus the muon momentum for fixed bins of the muon scattering angle. These kinematics correspond to the T2K experiment [1]. SuSAv2-MEC predictions are compared with data. Contrary to

the  $(e, e')$  cross sections shown in the previous section, here only the QE and 2p-2h MEC contributions are taken into account, as this is consistent with the analysis of T2K- $^{16}\text{O}$  data that is restricted to charged-current processes with no pions in the final state ( $\text{CC}0\pi$ ). We show the separate contributions of the pure QE, the 2p-2h MEC and the sum of both. Notice the role of the MEC effects compared with the pure QE ones — of the order of  $\sim 15\%$  at the maximum of the peak, except for forward angles, where they represent about 20% of the total cross section. Furthermore, the MEC peak compared with the QE one is shifted to smaller  $p_\mu$ -values. These results, which have already been observed in the case of T2K- $^{12}\text{C}$  (see [18]), are in contrast with the analysis of other experiments, namely, MiniBooNE and MINERvA, that show 2p-2h MEC relative effects to be larger and the peak location more in accordance with the QE maximum. This can be connected with the much narrower distribution presented by the T2K neutrino flux that explains the smaller 2p-2h MEC contribution and the location of its peak.

The SuSAv2-MEC approach provides predictions in good agreement with T2K data in most of the situations, although here 2p-2h MEC effects do not seem to improve in a significant way the comparison with data. This is at variance with other experiments, MiniBooNE and MINERvA, and it is connected with the minor role played by MEC. Notice that in most of the situations, both the pure QE and the total QE+MEC predictions describe data with equal success. A similar discussion was already presented in [18] for  $^{12}\text{C}$ .

Figure 4 compares the SuSAv2 CCQE to the SF calculation for the weighted cross section averaged over bins in scattering angle. Two versions of the SF calculation are shown, one that integrates over all possible values of the neutrino momentum and another that integrates over values for which  $\omega \geq 50\text{MeV}$  (see also the discussions concerning this strategy for exploring the sensitivities to the near-threshold region in the following section). Note that the fully integrated calculation is much larger than the SuSAv2 result at forward angles, but with the difference decreasing with increasing angle, becoming in reasonable agreement with SuSAv2 in the largest first angular bin. The cutoff SF result is smaller than SuSAv2 at forward angles, but comes into reasonable agreement as the angle increases. This is reason for some caution, since none of the CCQE models contains a complete description of inelastic scattering for ejected protons with kinetic energies below 50 MeV. Certainly this is the case for the PWIA SF model where plane-waves are involved and the near-threshold region cannot be successfully represented. Importantly, a large amount of the data collected

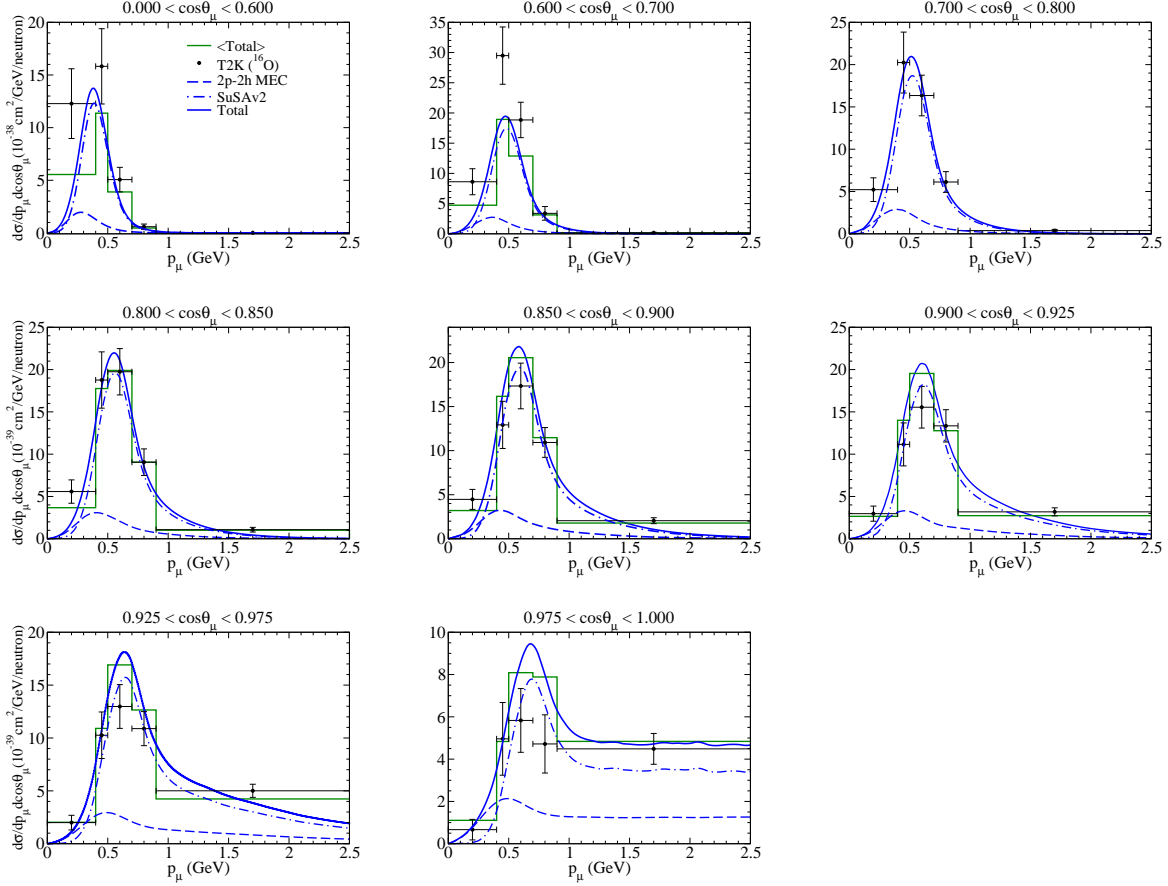


FIG. 3: (Color online) T2K flux-folded double differential cross section per target neutron for the  $\nu_\mu$  CCQE process on  $^{16}\text{O}$  displayed versus the muon momentum  $p_\mu$  for various bins of  $\cos\theta_\mu$  obtained within the SuSAv2-MEC approach. QE and 2p-2h MEC results are shown separately. The histogram represents the theoretical average of the total result over each bin of  $p_\mu$ . The data are from [1].

in the T2K experiment shown here falls into this region. The SuSAv2 approach involves an assumption which is discussed more fully in previous work where the ideas were developed about how so-called Pauli Blocking can be generalized from the only model where the concept is well-founded, namely, the extreme RFG model. The results obtained within the SuSAv2 approach are not in disagreement with the data, even at forward angles. However, one should still exercise some caution in drawing any final conclusions about how well one can claim to understand this region, *i.e.*, in any existing model. This problem deserves to be given greater attention in the future.

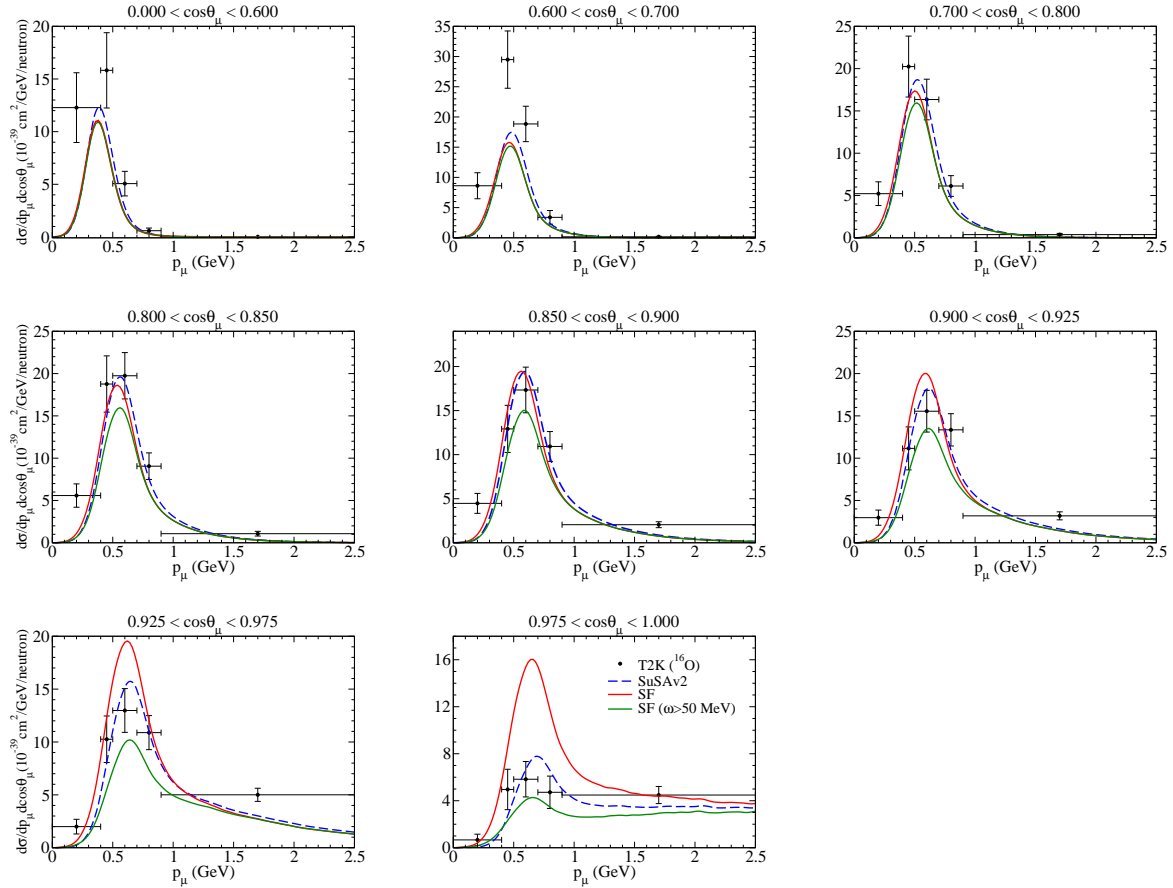


FIG. 4: (Color online) T2K flux-folded double differential cross section per target neutron for the  $\nu_\mu$  CCQE process on  $^{16}\text{O}$  displayed versus the muon momentum  $p_\mu$  for various bins of  $\cos\theta_\mu$  obtained within the SF model and the SuSAv2(QE) model. The contribution above  $\omega > 50$  MeV is also displayed for the SF model. The data are from [1].

### C. T2K: Oxygen versus Carbon

To make clear how nuclear effects enter in the analysis of the T2K experiment, in Fig. 5 we show the predictions provided by SuSAv2-MEC for the neutrino-averaged double differential cross sections per neutron in the cases of  $^{12}\text{C}$  (red lines) and  $^{16}\text{O}$  (blue). Here we show only the total results of adding the QE and MEC contributions, since the latter are essentially equal for carbon and oxygen when scaled by the number of neutrons in the two nuclei; the MEC contributions for carbon are thus essentially those shown for oxygen in Fig. 3. Although the scaling behaviors of the QE and the 2p2h cross sections are different — while the former goes like  $k_F^{-1}$  (scaling of the second kind), the latter increases as  $k_F^2$  — the results

in Fig. 5 are very similar for the two nuclei in most of the kinematical situations. This is a consequence of the very close values of  $k_F$  assumed in both cases, namely, 228 MeV/c (230) for  $^{12}\text{C}$  ( $^{16}\text{O}$ ). Only at forward angles (bottom panels) do some differences between the results for  $^{12}\text{C}$  and  $^{16}\text{O}$  emerge where the oxygen results are somewhat larger. Also, the amount of this difference increases as the scattering angle approaches zero. This behavior comes essentially from the QE response, since, as noted above, the MEC contributions for the two nuclei are very similar. It arises from the fact that at very forward angles the transferred energy in the process is very small and then the different values of  $E_{shift}$  for the two nuclei become significant. It should also be noted that in the last two panels the experimental angular bins are not exactly the same for the two nuclei. However, in spite of these potential sensitivities to small- $\omega$  dynamics, it is important to point out that the model is capable of reproducing the data for  $^{12}\text{C}$  and  $^{16}\text{O}$  within their error dispersion. As a test to evaluate the importance of having different  $E_{shift}$  values at low energies, these were set equal for the two nuclei and the effect goes away. Again, as stated above, the near-threshold region should be viewed with caution in all existing modeling.

We explore the dependence of the C/O differences upon the neutrino energy in a bit more detail by displaying in Fig. 6 the total integrated cross section per neutron with no neutrino flux included versus the neutrino energy. The results shown here indicate that nuclear effects between these nuclei in the total cross section, that is, including both the QE and 2p-2h MEC contributions, are very tiny, at most of the order of  $\sim 2\text{-}3\%$ . This minor difference is also observed for the pure QE response (slightly higher for carbon) and the 2p-2h MEC (larger for oxygen). This is connected with the differing scaling behavior shown by the QE and 2p-2h MEC responses with the Fermi momentum, and the very close values of  $k_F$  selected for the two nuclei. Upon including both the QE and 2p-2h MEC contributions, one observes that nuclear effects in the total cross section are very tiny. We also show the effect of making a “cut” at  $\omega = 50$  MeV, namely, setting any contribution from below this point to zero. This has been used in past work as a crude sensitivity test to ascertain the relative importance of the near-threshold region. If significant differences are observed when making the cut, then one should have some doubts about the ability of the present modeling (indeed, likely of all existing modeling) to successfully represent the cross section in this region. What we observe for the total cross section shown in the figure are relatively modest effects from near-threshold contributions, although one should be aware that this is

not so for differential cross sections at very forward angles where small- $\omega$  contributions can be relatively important, as discussed above.

Although not shown in Fig. 6 for simplicity, the use of a smaller value of  $k_F$  for  $^{16}\text{O}$ , as the one  $k_F = 216$  MeV/c considered in some previous work [24, 29, 33], leads to more significant differences in the QE (being larger) and 2p-2h MEC (smaller) contributions, but the total response remains rather similar to the result for  $^{12}\text{C}$ . It is important to point out that the use of different  $k_F$ -values only leads to significant discrepancies for low transferred energies, *i.e.*,  $\omega \leq 50$  MeV, a kinematical region where other ingredients, not included in the SuSAv2-MEC model, can be important. Moreover, the smaller the neutrino energy is the larger are the relative contributions coming from transfer energies below 50 MeV.

The results for the single-differential cross sections per neutron corresponding to the T2K experiment are presented in Fig. 7. Here we show the cross sections both versus the scattering angle and against the muon momentum using the values of the Fermi momentum given above, namely, 228 MeV/c ( $^{12}\text{C}$ ) and 230 MeV/c ( $^{16}\text{O}$ ). The separate contributions of the pure QE (dot-dashed), 2p-2h MEC (dashed) and the total result (solid) are shown. As noted, the differences seen between the two nuclei are very tiny. Then in Fig. 8 we show the same cross sections for oxygen obtained using two different values of  $k_F$ , namely, 230 and 216 MeV/c, to verify the statement made in Sec. II B that the results are typically relatively insensitive to variations of this magnitude.

Concerning the analysis of the role played by the nuclear effects, the uncertainty related to the use of different  $k_F$ -values is of the order of  $\sim 2\text{-}3\%$ . The analysis of the ratio  $^{16}\text{O}/^{12}\text{C}$  leads to differences below 3% except for the low-kinematic region where these figures are larger as a consequence of the high sensitivity to different parameters such as the effects arising from  $E_{shift}$  and the mass of the residual nucleus.

#### D. T2K antineutrino-water scattering

Finally, for completeness, in Fig. 9 we show the antineutrino-oxygen (*i.e.*, with no hydrogen contribution) and in Fig. 10 the antineutrino-water (*i.e.*, with the hydrogen contribution) CC double differential cross sections computed using the same model employed above for the neutrino-oxygen case. As observed, the relative contribution of the 2p-2h MEC contribution compared with the pure QE one is very similar to the case of neutrinos, also showing

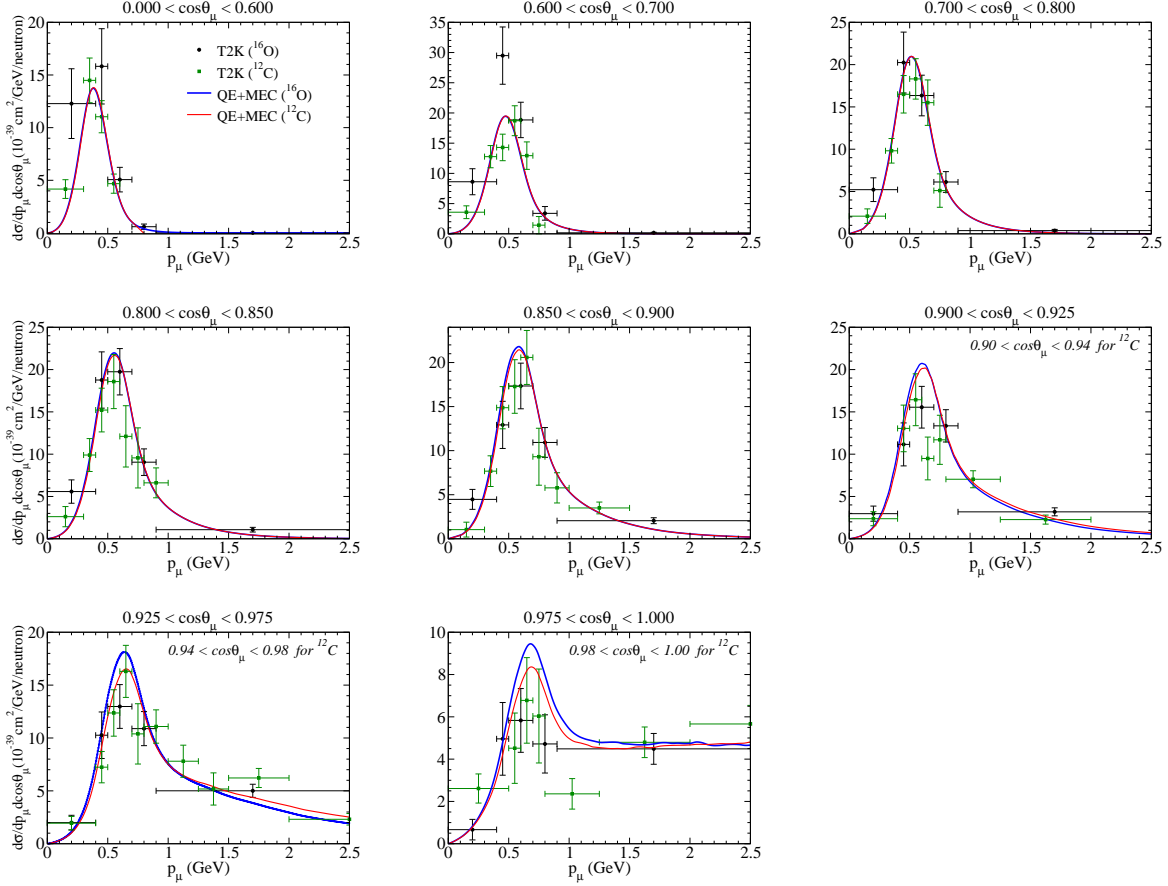


FIG. 5: (Color online) Similar to Fig. 3, but now including also the results corresponding to the T2K- $\nu_\mu$  CCQE process on  $^{12}\text{C}$ . The data are from [1, 41]

the same general shape versus the muon momentum. The SF antineutrino results using the same model as employed for neutrino reactions are also shown in the figures and display similar behavior to what was observed above.

#### IV. CONCLUSIONS

In the light of new results from the T2K collaboration on neutrino-oxygen CC $\nu$  cross sections we have employed our previous SuSAv2+MEC approach that had been developed for studies of neutrino-carbon CC $\nu$  cross sections to study the relative importance of the various ingredients in the model with respect to how they impact interpretations of the cross sections. This required two basic steps: (1) we first studied the rather limited database of results for inclusive electron scattering from oxygen to determine the (few) parameters

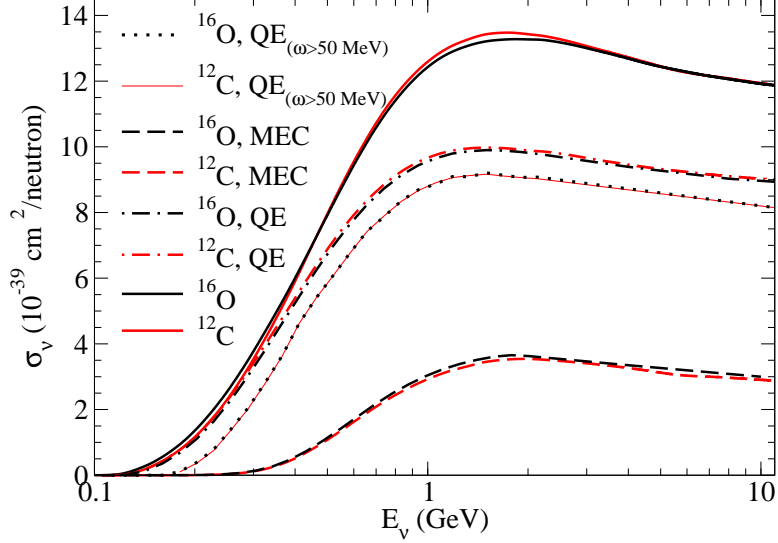


FIG. 6: (Color online) Total  $\nu_\mu$  cross section per nucleon as a function of the neutrino energy evaluated for  $^{12}\text{C}$  and  $^{16}\text{O}$  nuclei. Separate contributions of the pure QE (dot-dashed) and 2p-2h MEC (dashed). The effect of making a cut in  $\omega$  below 50 MeV for the QE contribution is also shown.

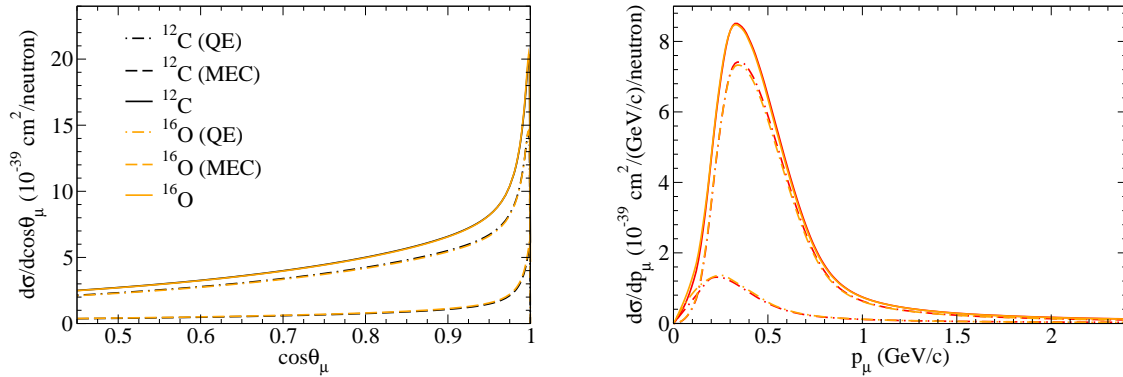


FIG. 7: (Color online). T2K flux-averaged CCQE neutrino differential cross sections per neutron for  $^{12}\text{C}$  and  $^{16}\text{O}$  as functions of the muon scattering angle (left panel) and of the muon momentum (right panel). The Fermi momenta here are 228 MeV/c for  $^{12}\text{C}$  and 230 MeV/c for  $^{16}\text{O}$ .

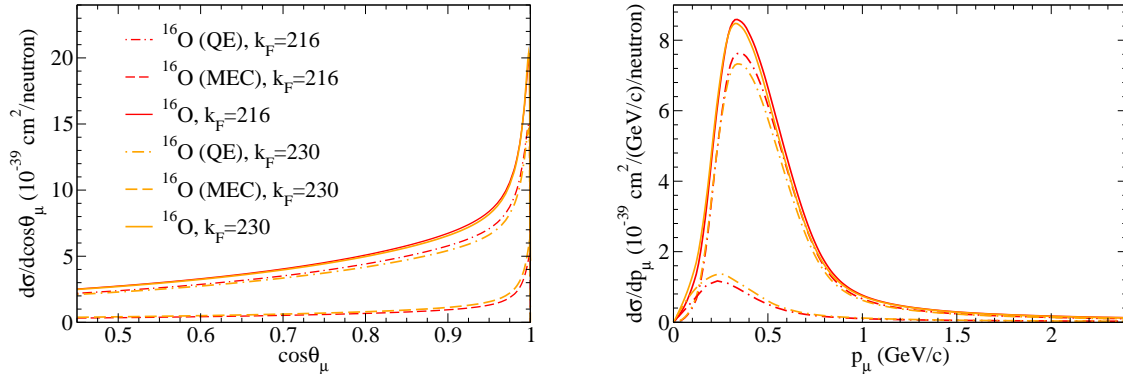


FIG. 8: (Color online). T2K flux-averaged CCQE neutrino differential cross sections per neutron for  $^{16}\text{O}$  as functions of the muon scattering angle (left panel) and of the muon momentum (right panel), showing the effect of choosing two values for  $k_F$  (in MeV/c) and  $E_{shift}$ , being the latter 16 MeV (20 MeV) for  $^{16}\text{O}$  ( $^{12}\text{C}$ ).

in the SuSAv2+MEC model, and (2) we extended the approach from studies of inclusive ( $e, e'$ ) reactions to inclusive  $CC\nu$  reactions in exactly the same way used in our previous analyses of carbon. Given some ambiguity in the choice of parameters we also explored the consequences of making different choices, for instance, of the parameter  $E_{shift}$  used in our approach. Additionally we inter-compared  $CC\nu$  results for oxygen and carbon to explore the robustness of attempts to deduce the cross sections for one from the other. Moreover, we have provided predictions for antineutrino-oxygen and antineutrino-water cross sections in advance of their being available from the T2K collaboration. Finally, we have also included QE inclusive electron scattering and  $CC\nu$  (neutrino and antineutrino) results using a spectral function for oxygen together with a factorized PWIA model for the reactions.

The results are very satisfying. We see that the SuSAv2+MEC approach agrees quite well with the data, having no significant disagreements given the uncertainties in the data. The SF model used in the present work provides results only for the QE contribution and, when one does a theory-to-theory comparison between this model and the SuSAv2 model for the QE contribution, one sees generally good agreement with the former lying somewhat lower than the latter. Such is expected, since the SuSAv2 model contains intrinsic transverse enhancement effects that are absent in most models, certainly in the PWIA SF model.

The main place where disagreements are observed is at very forward angles, namely at

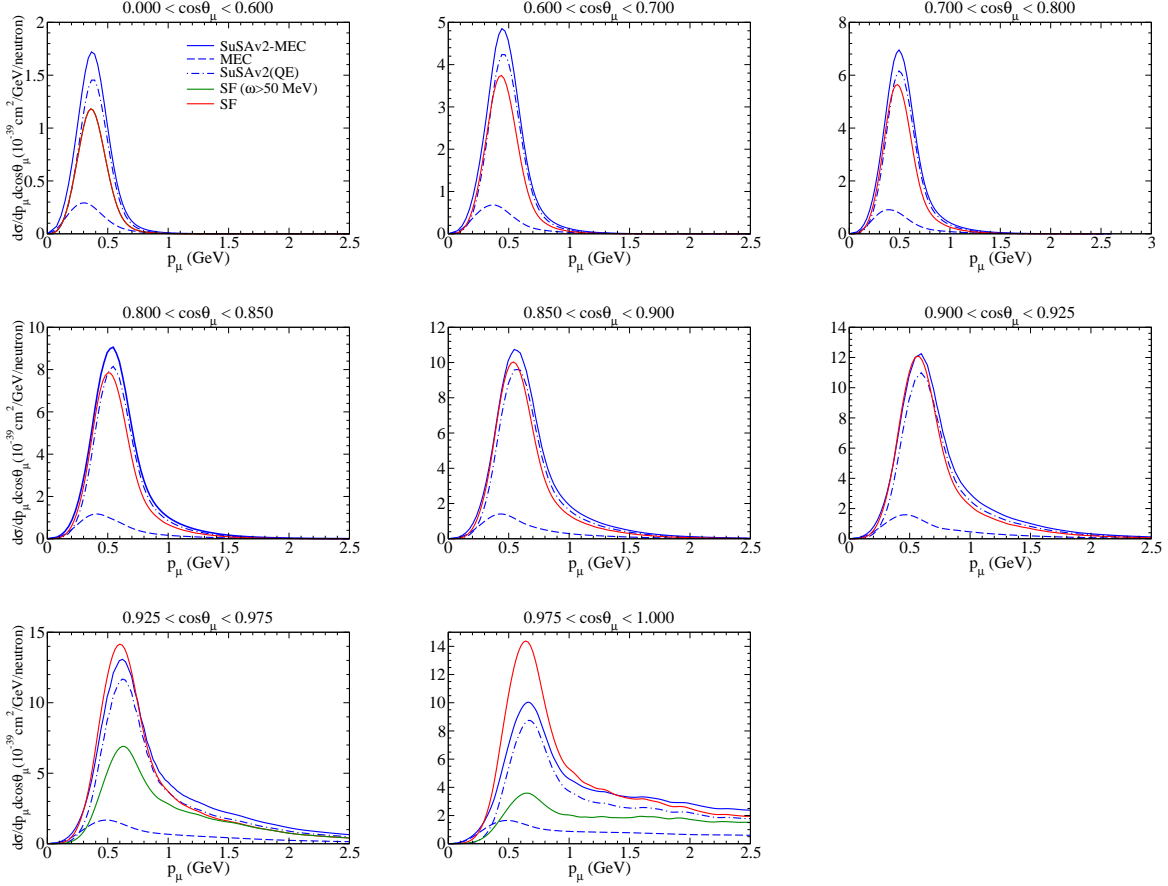


FIG. 9: (Color online) T2K flux-folded double differential cross section per target proton for the  $\bar{\nu}_\mu$  CCQE process on oxygen. The SF results are also displayed. In the last two panels the SF result corresponding to  $\omega > 50$  MeV is also shown (green curve).

rather low excitation energies. To test the sensitivity to this near-threshold region we do as we have in previous work and cut out all contributions from  $\omega < 50$  MeV: when nothing significant occurs one can conclude that these contributions are unimportant. However, when large changes are observed, we need to exercise caution in believing the modeling. For the SF model this forward-angle region shows very large effects, indicating, as should be expected, that the PWIA fails in the near-threshold region. In contrast, the SuSAv2 model contains an extension of what is usually called “Pauli blocking” and appears to do much better. Nevertheless, even for the latter approach some caution should be exercised.

Given the success of our modeling for inclusive  $(e, e')$  and  $CC\nu$  reactions now on two different nuclei we have increased confidence in employing the approach for heavier nuclei. New features are likely to emerge in these cases and presently we are beginning to explore

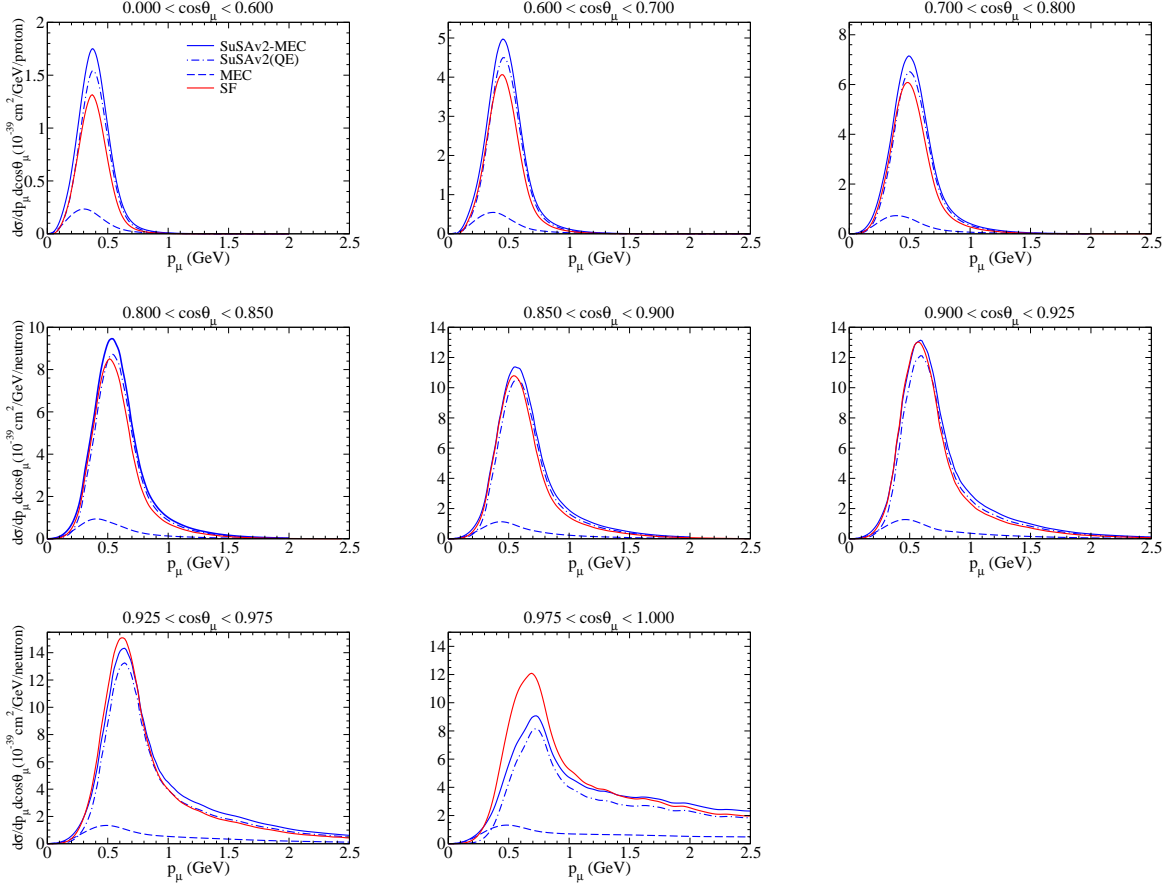


FIG. 10: (Color online) T2K flux-folded double differential cross section per target proton for the  $\bar{\nu}_\mu$  CCQE process on water. The SF results are also displayed.

their consequences. Finally, and this was part of the motivation for including the SF modeling in the present study, we are engaged in extending the scope of our studies to include semi-inclusive  $CC\nu$  reactions, and being able to ascertain the capabilities of the SF approach for inclusive scattering provides a benchmark for the semi-inclusive studies.

### Acknowledgments

This work has been partially supported by the Spanish Ministerio de Economía y Competitividad and ERDF (European Regional Development Fund) under contracts FIS2014-59386-P, FIS2014-53448-C2-1, by the Junta de Andalucía (grants No. FQM-225, FQM160), by the INFN under project MANYBODY, by the University of Turin under contract BARM-RILO-17, and part (TWD) by the U.S. Department of Energy under cooperative agree-

ment DE-FC02-94ER40818. IRS acknowledges support from a Juan de la Cierva fellowship from MINECO (Spain). GDM acknowledges support from a Junta de Andalucía fellowship (FQM7632, Proyectos de Excelencia 2011). JWVO acknowledges support by the US Department of Energy under Contract No. DE-AC05-06OR23177, and by the U.S. Department of Energy cooperative research agreement DE-AC05-84ER40150. We thank Omar Benhar for providing the oxygen spectral function. We acknowledge useful discussions during the “Two-body current contributions in neutrino-nucleus scattering” ESNT workshop at CEA-Saclay, April 2016. We thank Sara Bolognesi (IRFU, SPP, CEA-Saclay) for her active participation on discussions of experimental issues.

- 
- [1] K. Abe et al. (T2K Collaboration), arXiv:1708.06771 (2017).
  - [2] M. Martini, M. Ericson, G. Chanfray, and J. Marteau, *Phys. Rev. C* **80**, 065501 (2009).
  - [3] J. E. Amaro, M. B. Barbaro, J. A. Caballero, T. W. Donnelly, and C. F. Williamson, *Phys. Lett. B* **696**, 151 (2011).
  - [4] J. Nieves, I. Ruiz Simo, and M. J. Vicente Vacas, *Phys. Lett. B* **707**, 72 (2012).
  - [5] J. Nieves, I. Ruiz Simo, and M. J. Vicente Vacas, *Phys. Lett. B* **721**, 90 (2013).
  - [6] K. Gallmeister, U. Mosel, and J. Weil, *Phys. Rev. C* **94**, 035502 (2016).
  - [7] O. Lalakulich, K. Gallmeister, and U. Mosel, *Phys. Rev. C* **86**, 014614 (2012).
  - [8] O. Lalakulich, U. Mosel, and K. Gallmeister, *Phys. Rev. C* **86**, 045606 (2012).
  - [9] G. D. Megias, J. E. Amaro, M. B. Barbaro, J. A. Caballero, and T. W. Donnelly, *Phys. Rev. D* **94**, 013012 (2016).
  - [10] I. Ruiz Simo, C. Albertus, J. E. Amaro, M. B. Barbaro, J. A. Caballero, and T. W. Donnelly, *Phys. Rev. D* **90**, 033012 (2014).
  - [11] V. Pandey, N. Jachowicz, M. Martini, R. González-Jiménez, J. Ryckebusch, T. Van Cuyck, and N. Van Dessel, *Phys. Rev. C* **94**, 054609 (2016).
  - [12] I. Ruiz Simo, J. E. Amaro, M. B. Barbaro, A. De Pace, J. A. Caballero, G. D. Megias, and T. W. Donnelly, *Phys. Lett. B* **762**, 124 (2016).
  - [13] A. Meucci and C. Giusti, *Phys. Rev. D* **85**, 093002 (2012).
  - [14] A. Meucci, M. B. Barbaro, J. A. Caballero, C. Giusti, and J. M. Udias, *Phys. Rev. Lett.* **107**, 172501 (2011).

- [15] J. E. Amaro, M. B. Barbaro, J. A. Caballero, T. W. Donnelly, A. Molinari, and I. Sick, *Phys. Rev. C* **71**, 015501 (2005).
- [16] R. González-Jiménez, G. D. Megias, M. B. Barbaro, J. A. Caballero, and T. W. Donnelly, *Phys. Rev. C* **90**, 035501 (2014).
- [17] G. D. Megias, T. W. Donnelly, O. Moreno, C. F. Williamson, J. A. Caballero, R. González-Jiménez, A. De Pace, M. B. Barbaro, W. M. Alberico, M. Nardi, et al., *Phys. Rev. D* **91**, 073004 (2015).
- [18] G. D. Megias, J. E. Amaro, M. B. Barbaro, J. A. Caballero, T. W. Donnelly, and I. Ruiz Simo, *Phys. Rev. D* **94**, 093004 (2016).
- [19] J. E. Amaro, M. B. Barbaro, J. A. Caballero, A. De Pace, T. W. Donnelly, G. D. Megias, , and I. Ruiz Simo, *Phys. Rev. C* **95**, 065502 (2017).
- [20] O. Benhar, A. Fabrocini, S. Fantoni, and I. Sick, *Nucl. Phys.* **A579**, 493 (1994).
- [21] O. Benhar, N. Farina, H. Nakamura, M. Sakuda, and R. Seki, *Phys. Rev.* **D72**, 053005 (2005).
- [22] J. W. Van Orden, T. W. Donnelly, and O. Moreno (2017), 1707.04121.
- [23] T. Katori and M. Martini, *Journal of Physics G: Nuclear and Particle Physics* , **in press** (2017), arXiv:1611.07770 [hep-ph], URL <http://iopscience.iop.org/article/10.1088/1361-6471/aa8bf7>.
- [24] J. A. Caballero, *Phys. Rev. C* **74**, 015502 (2006).
- [25] V. Pandey, N. Jachowicz, T. V. Cuyck, J. Ryckebusch, and M. Martini, *Phys. Rev. C* **92**, 024606 (2015).
- [26] R. Gran, J. Nieves, F. Sánchez, and M. J. Vicente Vacas, *Phys. Rev. D* **88**, 113007 (2013).
- [27] A. Gil, J. Nieves, and E. Oset, *Nucl. Phys.* **A627**, 543 (1997).
- [28] D. B. Day, J. S. McCarthy, T. W. Donnelly, and I. Sick, *Annu. Rev. Nucl. Part. Sci.* **40**, 357 (1990).
- [29] J. E. Amaro, M. B. Barbaro, J. A. Caballero, T. W. Donnelly, and C. Maieron, *Phys. Rev. C* **71**, 065501 (2005).
- [30] M. Anghinolfi et al., *Nucl. Phys.* **A602**, 405 (1996).
- [31] J. S. O'Connell et al., *Phys. Rev.* **C35**, 1063 (1987).
- [32] C. Maieron, T. W. Donnelly, and I. Sick, *Phys. Rev. C* **65**, 025502 (2002).
- [33] J. A. Caballero, J. E. Amaro, M. B. Barbaro, T. W. Donnelly, C. Maieron, and J. M. Udías, *Phys. Rev. Lett.* **95**, 252502 (2005).

- [34] J. E. Amaro, M. B. Barbaro, J. A. Caballero, T. W. Donnelly, and J. M. Udías, Phys. Rev. C **75**, 034613 (2007).
- [35] R. González-Jiménez, M. V. Ivanov, M. B. Barbaro, J. A. Caballero, and J. M. Udias, Phys. Lett. B **718**, 1471 (2013).
- [36] J. A. Caballero, J. E. Amaro, M. B. Barbaro, T. W. Donnelly, and J. M. Udías, Phys. Lett. B **653**, 366 (2007).
- [37] J. W. Van Orden and T. W. Donnelly, Annals Phys. **131**, 451 (1981).
- [38] A. De Pace, M. Nardi, W. M. Alberico, T. W. Donnelly, and A. Molinari, Nucl. Phys. A **741**, 249 (2004).
- [39] K. Abe et al. (T2K Collaboration), Phys. Rev. D **87**, 092003 (2013).
- [40] K. Abe et al. (T2K Collaboration), Phys. Rev. Lett. **113**, 241803 (2014).
- [41] K. Abe et al. (T2K Collaboration), Phys. Rev. D **93**, 112012 (2016).
- [42] O. Benhar, D. Day, and I. Sick, Rev. Mod. Phys. **80**, 189 (2008).
- [43] M. Gari and W. Krupelmann, Z. Phys. A **322**, 689 (1985).
- [44] P. E. Bosted and M. E. Christy, Phys. Rev. C **77**, 065206 (2008).
- [45] A. M. Ankowski, M. B. Barbaro, O. Benhar, J. A. Caballero, C. Giusti, R. González-Jiménez, G. D. Megias, and A. Meucci, Phys. Rev. **C92**, 025501 (2015).